Time-Domain Aeroelastic Simulation on Stationary Body-Conforming Grids with Small Perturbation Boundary Conditions

Shuchi Yang*, Feng Liu†, Shijun Luo‡
Department of Mechanical and Aerospace Engineering
University of California, Irvine, CA 92697-3975

Her-Mann Tsai§
Temasek Laboratories
National University of Singapore
Kent Ridge Crescent, Singapore 119260

David M. Schuster¶
Aeroelasticity Branch
NASA Langley Research Center, Hampton, VA 23681

Small perturbation boundary conditions are formulated for solving the unsteady Euler equations on body-conforming stationary grids. The CFD solver with the approximate boundary conditions is coupled with elastic equations to predict the aeroelastic properties of airfoils. The accurate nonlinear Euler equations are solved in the field, while the movement of the solid surfaces is accounted for in the new boundary conditions without moving or deforming the computational grids. The first-order wall boundary conditions are used in solving the full Euler equations for steady, unsteady and aeroelastic cases, and the results are compared with Euler solutions with full boundary conditions on moving grids and known experimental data. The relative errors are analyzed quantitatively due to the variation of thickness or pitching angles of the airfoils for steady cases. Compared to a similar approximate boundary condition method on pure Cartesian grids, the present method on body-fitted grids eliminates the thickness limitation and the singularity at the leading edge of a round-nosed airfoil. It is shown that the simple first-order boundary conditions are adequate to represent airfoils with small deformation of both steady and unsteady cases.

I. Introduction

One of the difficulties in the time-domain simulation of flutter by using the Euler or Reynolds-Averaged Navier-Stokes equations is in generating a deforming grid around the moving structural components at every time step in the unsteady computation. In this respect, the conventional doublet-lattice method and the Transonic-Small-Disturbance potential flow method implemented in the NASA Langley CAP-TSD[1–3] code offers a significant advantage in terms of computer and user time because of the use of simple stationary grids. In an effort to take advantage of the use of a stationary Cartesian grid while eliminating the limitations of the small-perturbation potential model, Gao, Luo, Liu, and Schuster[4,5] presented an unsteady Euler method using stationary Cartesian grid for thin airfoils. The full unsteady boundary condition on the airfoil is approximated by using first-order expansion at the airfoil mean chord, which is placed on a grid line. Although such "a small-perturbation" approximation for the boundary conditions is only valid for thin airfoils, the flow model is not limited to small perturbations. For example, the computations will still be valid for flows at high angles of attack as long as the airfoil is thin. Results shown in Ref. 4 prove validity of the method for a range of flow conditions. However, because of the thin airfoil assumption, the accuracy deteriorates for thick airfoils. In addition a singularity exists at the leading edge of a blunt airfoil. In order to remove this singularity and the restriction of thin airfoils, so that the method may be extended to accurately treat thick wings and wing-body combinations, we propose in this paper an approximate boundary condition method on the nominal non-deformed air-

*Post-Doctoral Researcher.

†Professor. Associate Fellow AIAA.

‡Researcher.

§Principal Research Scientist. Member AIAA.

¶Senior Research Engineer. Associate Fellow AIAA.

foil with a body-conforming curvilinear grid. The full boundary conditions for the Euler equations on the moving airfoil are replaced by approximate boundary conditions on the stationary grid around the undeformed airfoil at its mean position by using Taylor expansions. Since the deformation or displacement of the airfoil from its original position is usually small in an aeroelastic problem, in particular, flutter simulations, we anticipate small errors by using such a simulation on a stationary grid, which can simply be the same grid used in the steady aerodynamic calculations.

An examination of the literature reveals that the approximate boundary condition method proposed here resembles the transpiration velocity method presented by Sankar, Malone, and Tassa[6] for the potential equation, and Sankar, Malone, and Schuster[7] and Fisherand Arena[8]for the Euler equations. However the present approach is based a Taylor series expansion of the full boundary conditions rather than a transpiration velocity concept. The Taylor expansion approach is capable of being extended to higher order accuracy. We also attempt to quantify the errors of the approximate boundary condition method systematically in terms of the amount of deformation in body thickness and rotation angle for steady and unsteady flows.

The formulation of the proposed approximate boundary conditions is presented first. They are implemented in a three-dimensional body-fitted grid code, PARCAE(PARallel Computation of AeroElasticity)[9] developed at UCI. Numerical examples for steady, unsteady and aeroelastic cases are given and results are compared with those obtained by the original PARCAE and the published experimental data. Discussions and conclusions are finally drawn.

II. Governing Equations

The two-dimensional unsteady Euler equations in conservative integral form in the Cartesian coordinate system (x, y) are

$$\frac{\partial}{\partial t}\int_V \mathbf{W}dV + \int_S \mathbf{G}\cdot\mathbf{n}dS = 0 \tag{1}$$

where

$$\mathbf{W} = \begin{bmatrix} \rho \\ \rho u \\ \rho v \\ \rho E \end{bmatrix} \tag{2}$$

$$\mathbf{G} = \begin{bmatrix} \rho(\mathbf{q}-\mathbf{q}_b) \\ \rho u(\mathbf{q}-\mathbf{q}_b) + p\mathbf{e}_x \\ \rho v(\mathbf{q}-\mathbf{q}_b) + p\mathbf{e}_y \\ \rho E(\mathbf{q}-\mathbf{q}_b) + p(u\mathbf{e}_x + v\mathbf{e}_y) \end{bmatrix} \tag{3}$$

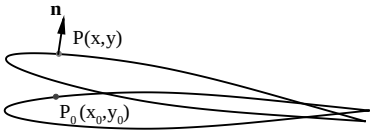

Fig. 1 Description of the movement of the airfoil.

$$\mathbf{q} = u\mathbf{e}_x + v\mathbf{e}_y \tag{4}$$

$$\mathbf{q}_b = u_b\mathbf{e}_x + v_b\mathbf{e}_y \tag{5}$$

$$E = \frac{1}{\gamma-1}\frac{p}{\rho} + \frac{1}{2}(u^2+v^2) \tag{6}$$

$$H = E + \frac{p}{\rho} \tag{7}$$

Following the procedure by Liu and Jameson,[10] a cell-centered finite volume method and Runge-Kutta multi-step scheme are used for the space discretization and time marching separately. Scalar and matrix artificial dissipation schemes are used to prevent oscillations near stagnation points and shock waves. In order to accelerate the computation, local time step and multi-grid are implemented. For unsteady cases, dual time-stepping is used to do the fully implicit time marching.[11]

III. Simplified Boundary Conditions

For an airfoil with small deformation or rotation, the original airfoil and the new position are considered as shown in Fig. 1. An arbitrary point $P_0(x_0,y_0)$ on the original airfoil moves to a new position P(x,y). For unsteady computation, the velocity boundary condition at P should be

$$\mathbf{q}\cdot\mathbf{n} = \mathbf{q}_b\cdot\mathbf{n} \tag{8}$$

where $\mathbf{q}_b$ is the velocity of the airfoil for unsteady cases and $\mathbf{n}$ is the unit normal vector at P. Using Taylor expansion, the flow variables at P can be represented by those at P_0:

$$\mathbf{q}(x,y) = \mathbf{q}(x_0,y_0) + \frac{\partial\mathbf{q}}{\partial x}(x_0,y_0)(x-x_0) + \frac{\partial\mathbf{q}}{\partial y}(x_0,y_0)(y-y_0) + O(\Delta r^2) \tag{9}$$

If the deformation of the airfoil is small, which means that $\Delta r = \sqrt{(x-x_0)^2+(y-y_0)^2} \ll 1$. With first-order approximation, we have

$$\mathbf{q}(x,y) = \mathbf{q}(x_0,y_0) + O(\Delta r) \tag{10}$$

Then equation (8) can be written as

$$\mathbf{q}(x_0,y_0)\cdot\mathbf{n} = \mathbf{q}_b\cdot\mathbf{n} \tag{11}$$

We can transform the above equation to a local grid coordinate system (ξ,η), and use the contravariant velocity (U,V). The relation between (U,V) and (u,v) is

$$\begin{aligned} u &= x_\xi U + x_\eta V \\ v &= y_\xi U + y_\eta V \end{aligned} \tag{12}$$

Substituting equation (12) to equation (11), we get the following approximate wall boundary condition.

$$V = -\frac{U(x_\xi n_x + y_\xi n_y) - (u_b n_x + v_b n_y)}{(x_\eta n_x + y_\eta n_y)} \tag{13}$$

Notice in the above equation, although the flow velocities are evaluated at the stationary position P_0, the normal vector $\mathbf{n}$ is evaluated at the actual point P, which changes with time. In addition u_b and v_b, the local body velocity components, are also time dependent in an unsteady motion.

In the same way, we can deal with the normal momentum equation, which is used to compute the pressure on the wall.

$$\mathbf{n}\cdot[\frac{\partial\mathbf{q}}{\partial t} + (\mathbf{q}\cdot\nabla)\mathbf{q}] = \mathbf{n}\cdot(-\frac{\nabla p}{\rho}) \tag{14}$$

Since we are using first-order approximation in this paper, we use the zero-th-order extrapolation to get the pressure on the wall from the first interior grid cells for both accurate and simplified boundary condition computations.

The above first-order approximation reduces to the transpiration velocity method[6–8] except for possible differences in the details of numerical implementation. However, the present Taylor series expansion approach allows us to attain higher order accuracy when needed.

IV. Results

A. Steady Cases

Before we implement the simplified boundary conditions for aeroelastic computations, several steady cases are tested in the following subsections.

A..1 Airfoil thickness effect

In order to validate the small disturbance boundary conditions for airfoil deformation, a grid for the NACA0012 airfoil is used to simulate the flow field around other NACA 4-digital airfoils whose thickness ratios range from 0.06 to 0.18. The computational grid is an O-type grid with 161×33 grid points.

Consider a subsonic case with a Mach number of 0.4 and an angle of attack of 2 degrees. Figure 2 shows the pressure contours for the NACA0008 airfoil computed on a grid around a NACA0012 airfoil as compared to those computed directly on the NACA0008 airfoil with the accurate full boundary conditions. There are slight differences between the two solutions in the flow field. Figure 3 shows the comparison of the surface pressure distributions from the two different treatments of the boundary conditions. We can see the pressure distributions on the wall are almost the same.

Next, consider a transonic case with a Mach number of 0.8 and an angle of attack of 2 degrees. Figures 4 and 5 show the comparisons of the pressure contours and the surface pressure distributions between the solutions for the NACA0016 airfoil. The solid lines represent the solutions obtained using a grid around NACA0016 with the full boundary conditions and the dash lines represent those obtained with the small disturbance boundary conditions on a grid around the NACA 0012 airfoil. Although the thickness perturbation in this transonic case is the same 4% as in the previous subsonic case, the difference between the approximate solution and the exact solution for this case is noticeably greater than that in the subsonic case. In order to quantify this behavior, Figure 6 shows the relative errors between the solutions of the simplified boundary conditions with the NACA0012 grid and those from the full boundary conditions with its own grid for various thickness ratios. The relative error is defined as:

$$\varepsilon = \frac{\int |(Cp)_{SBC} - (Cp)_{ABC}|\,dx}{\int |(Cp)_{ABC}|\,dx} \tag{15}$$

The subscript ABC means the solutions predicted with the accurate boundary conditions and SBC means the solutions predicted with simplified boundary conditions.

The errors vary almost linearly with the variation of thickness ratios. It is also clear that the relative errors are greater for transonic flows than those for subsonic flows.

A..2 Airfoil rotation

Another test case is to validate the small disturbance boundary conditions for airfoil rotation. Consider the steady flow field past an NACA0012 airfoil

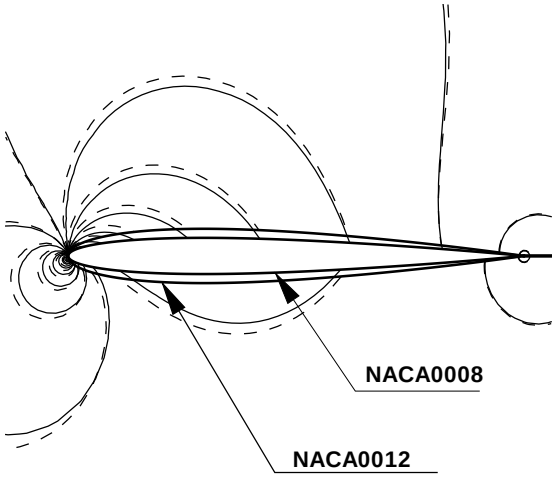

Fig. 2 Pressure contours for NACA0008 with different grids and boundary conditions, $M_\infty = 0.40$, $\alpha = 2.0$ degrees (Solid lines represent the results with accurate boundary conditions and dash lines represent results with simplified boundary conditions).

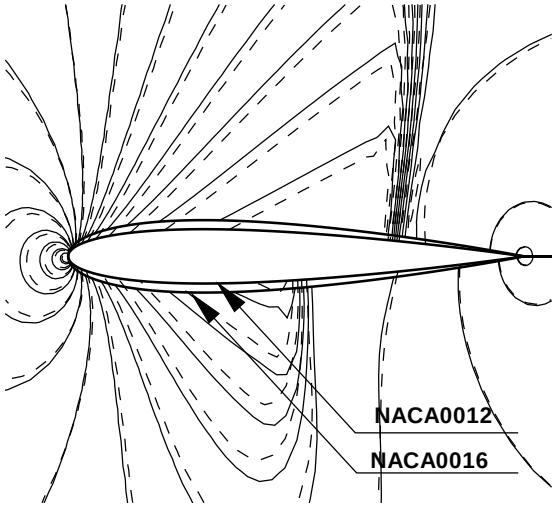

Fig. 4 Pressure contours for NACA0016, $M_\infty = 0.80$, $\alpha = 2.0$ degrees (Solid lines represent the results with accurate boundary conditions and dash lines represent results with simplified boundary conditions).

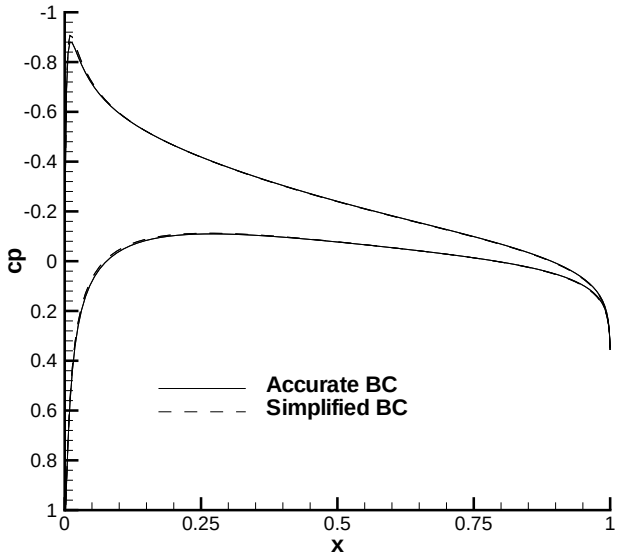

Fig. 3 Pressure distribution for NACA0008 with different grids and boundary conditions $M_\infty = 0.40$, $\alpha = 2.0$ degrees.

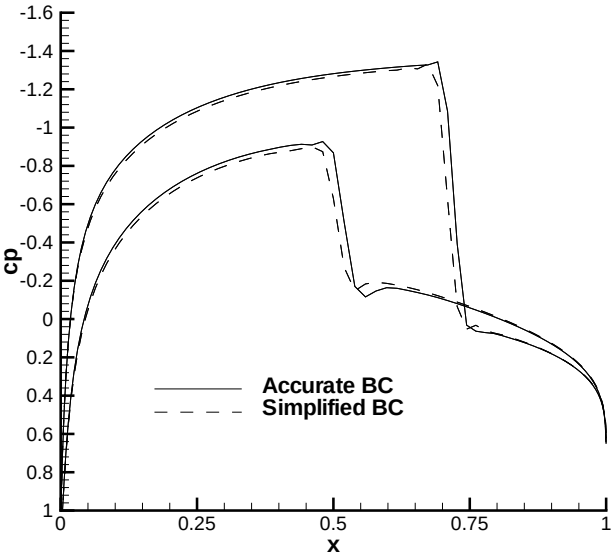

Fig. 5 Pressure distribution for NACA0016, $M_\infty = 0.80$, $\alpha = 2.0$ degrees.

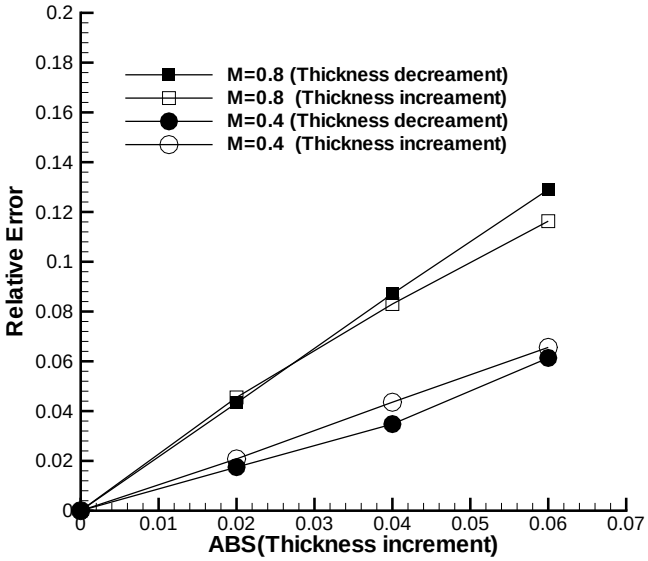

Fig. 6 Variation of relative error versus the thickness variation.

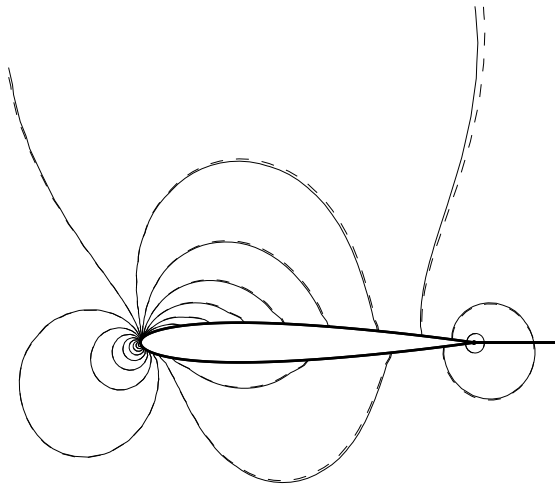

Fig. 7 Pressure contours for NACA0012, $M_\infty = 0.40$, α=2.0 degrees (Solid lines represent the results with accurate boundary conditions and dash lines represent results with simplified boundary conditions).

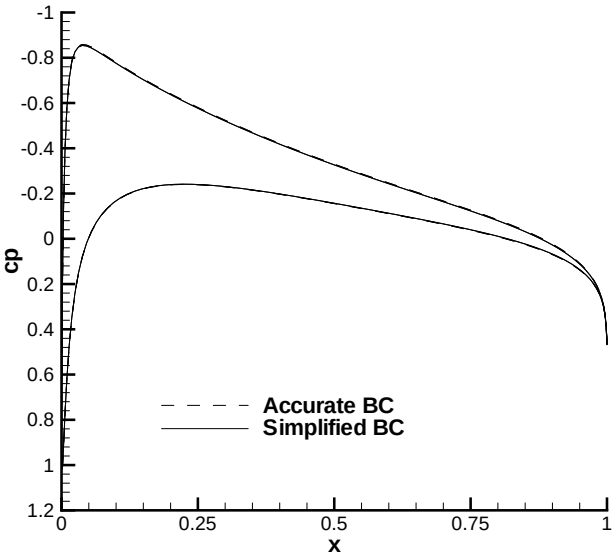

Fig. 8 Pressure distribution for NACA0012, $M_\infty = 0.40$, α=2.0 degrees.

that is pitched up by an angle α relative to a horizontal free stream. We would like to compute the solution by using the proposed approximate boundary condition method on the same grid as used in the above thickness studies with the airfoil lying in parallel with the horizontal free stream. For this case, the accurate solution with the full boundary conditions can be obtained simply by either rotating the airfoil and the grid by α degrees or more simply setting the free stream flow angle to α degrees. Figures 7 and 8 show the comparisons of the pressure contours and the surface pressure distribution, respectively, of the approximate and the accurate solutions for the subsonic case with a free stream Mach number of 0.4 and a 2 degree airfoil rotation angle. The two solutions almost overlap each other for this Mach number. Figures 9 and 10 show the same comparisons when the free stream Mach number is increased to 0.8 while the airfoil rotation is kept at 2 degrees. There are slight but noticeable differences between the two solutions. The shock wave position predicted by the approximation method is slightly downstream of that by the full boundary condition method.

To quantify the effect of rotation angle, the same relative error defined by Eqn. (15) is calculated and plotted in Fig. 11 for a number of rotation angles at Mach numbers 0.4 and 0.8. Similar to the result shown in Fig. 6, the relative error behaves linearly with the airfoil rotation angle, consistent with the first-order expansion of the boundary conditions. The constant of proportionality in this linear dependence is greater for transonic flows than for subsonic flows.

B. Unsteady Computation

The present approximate method is used to calculate the flow over an NACA64A010 airfoil pitching around its quarter-chord point. The unsteady case from Ref. 12 is computed and compared with the experimental data. The pitching motion of the airfoil is

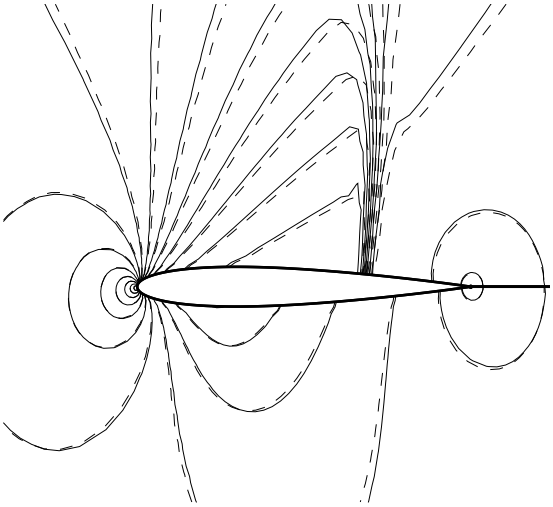

Fig. 9 Pressure contours for NACA0012,M_∞ = 0.80, α=2.0 degrees (Solid lines represent the results with accurate boundary conditions and dash lines represent results with simplified boundary conditions).

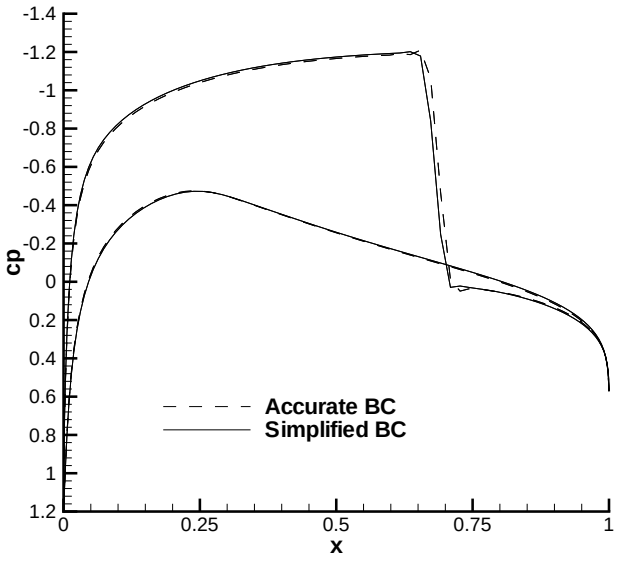

Fig. 10 Pressure distribution for NACA0012,M_∞ = 0.80, α=2.0 degrees.

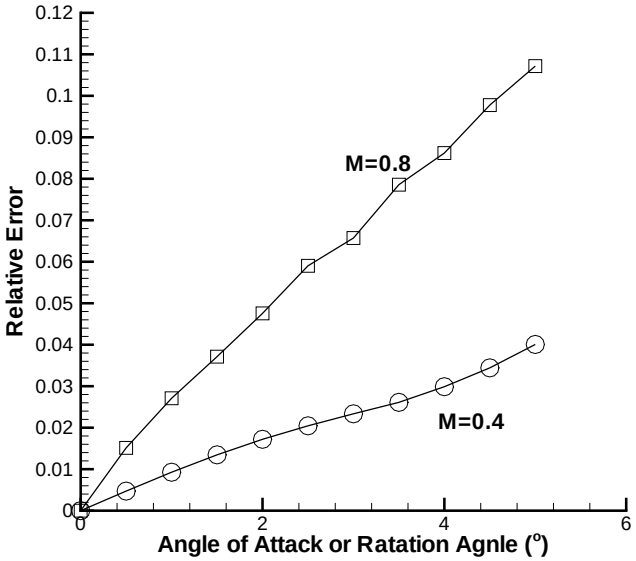

Fig. 11 Relative error versus the rotation angle of NACA0012.

described by the following equation.

$$\alpha(t) = \alpha_m + \alpha_0 \sin \omega t \tag{16}$$

where ω, α_m and α_0 are constants. The angular frequency ω is related to the reduced frequency defined as

$$\kappa = \frac{\omega c}{2U_\infty} \tag{17}$$

The AGARD CT case 55 of Ref. 12 is studied. The airfoil pitches at the free stream Mach number M_∞=0.796 and α_m=0.0 degrees, α_0 = 1.01 degrees, and κ=0.202. The surface pressure coefficients are represented in their Fourier components. Figures 12 and 13 present the comparison of the real and imaginary parts of the first, second and third modes. In these figures, the surface pressure distribution of the first mode agrees well with the experimental result. The shock position and the stagnation pressure are predicted accurately. For the second mode and third modes, there are some differences, but the results of the simplified boundary conditions and the accurate boundary conditions coincide with each other.

In order to quantitatively estimate the accuracy of the simplified boundary conditions for unsteady computations, a series of unsteady computations are tested with different amplitudes of pitching. In equation (16), α_m is set to 0 and α_0 is varied from 0 to 20 degrees. The unsteady lift coefficients are expressed as their Fourier components. Figure 14 shows the comparison of the amplitude and phase angle of the first mode only

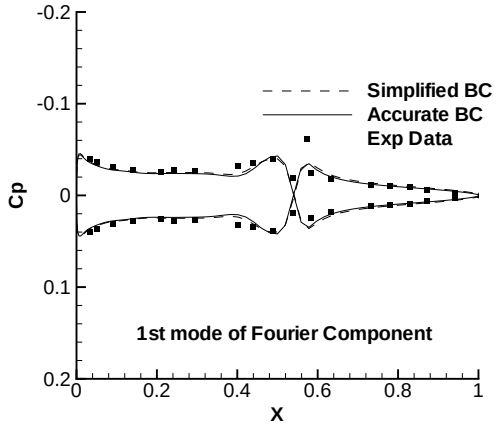

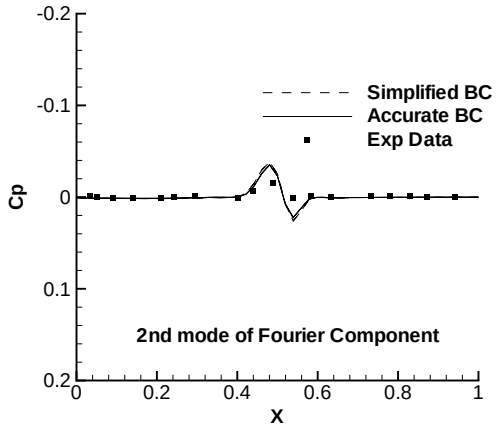

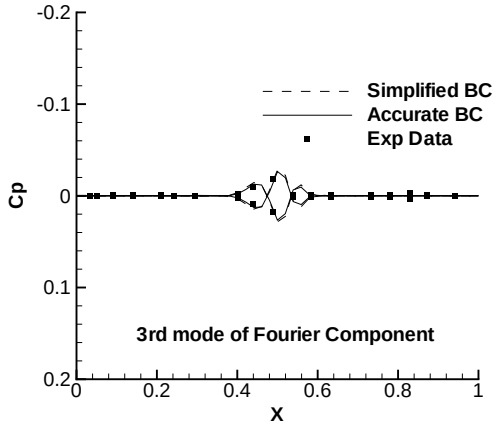

Fig. 12 Comparison of computational surface pressure distribution of NACA64A010 with experimental data, $M_\infty = 0.796$, $\alpha_m = 0.0$ degrees, $\alpha_0 = 1.01$ degrees, $\kappa = 0.202$ (Real part) .

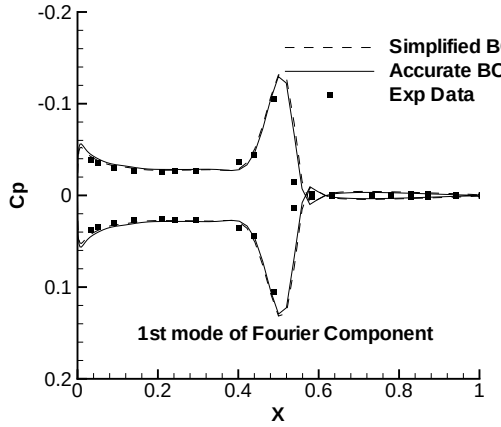

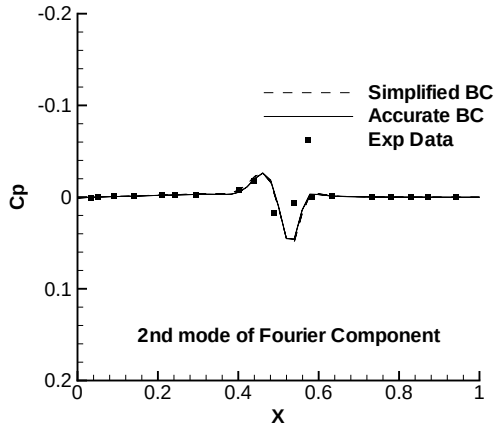

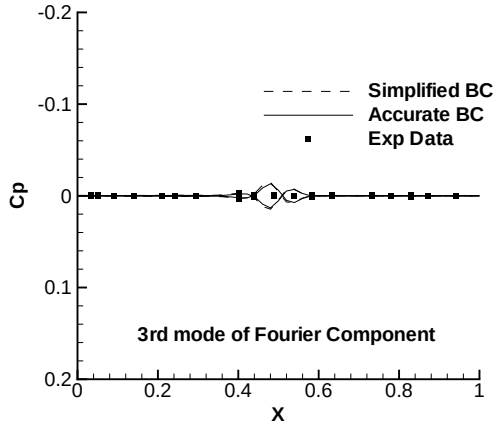

Fig. 13 Comparison of computational surface pressure distribution of NACA64A010 with experimental data, $M_\infty = 0.796$, $\alpha_m = 0.0$ degrees, $\alpha_0 = 1.01$ degrees, $\kappa = 0.202$ (Imaginary part).

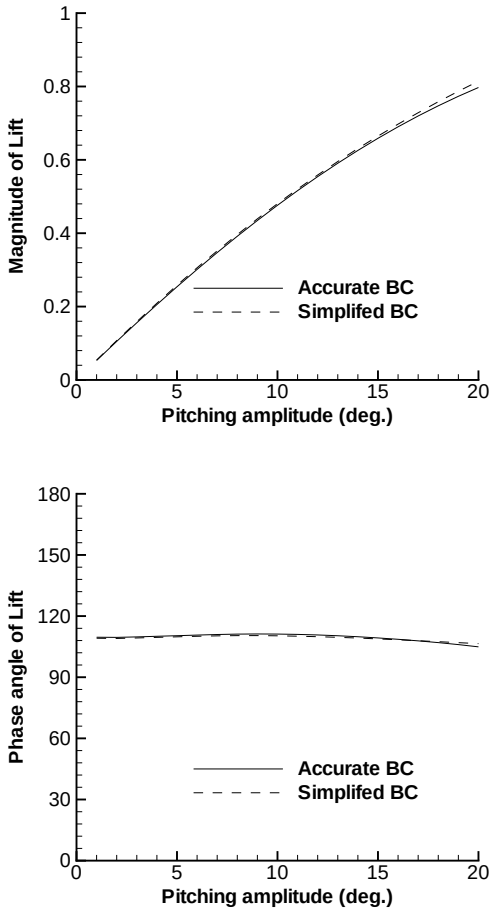

Fig. 14 Comparison of first mode of lift coefficients versus the amplitude of the pitching for NACA64A010, $M_\infty = 0.796$**,** $\kappa = 0.202$**.**

since the amplitudes of the second and higher modes are much smaller. The difference of the amplitude is less than 3 percent even with 20 degree angle of attack and the phase difference is very small, too. This is a pleasant surprise as it shows that the approximate boundary condition method yields much better accuracy for unsteady computations than for steady flows. On examination of the approximations made in the simplified boundary conditions, however, this improvement in accuracy for unsteady flows is not accidental. The unsteady effect due to the velocity of the airfoil surface velocity u_b, v_b and also the normal vector $\mathbf{n}$ are exactly represented in Eq. (13).

C. Aeroelastic Computation

We use the current unsteady Euler solver in a coupled CFD-CSD method[13] for the two-dimensional Isogai wing model,[14,15] Case A. This model simulates the bending and torsional motion of a wing cross-section in the outboard portion of a swept wing. It consists of two degrees of freedom, plunging and pitching, for a NACA 64A010 airfoil. We will compute the case with the current Euler equations and compare the results in Ref. 13. The details of the structural model can be found in Ref. 16 as well as in Refs. 14 and 15. The case whose mass ratio μ= 60 is considered.

In order to compute the flutter boundary, different values of speed index V_f are tested. V_f is defined as

$$V_f = \frac{U_\infty}{b\omega\sqrt{\mu}} \tag{18}$$

where ω is the lowest natural frequency of the structure, μ is the mass ratio, b is the airfoil half chord.

Figures 15, 16, and 17 show the time histories of pitching and plunging movement of the airfoil at the Mach number of 0.75. At V_f=1.00, Fig. 15 shows that both the plunging and pitching motion decays with time, which indicates that the aeroelastic system is stable for this V_f. For a higher V_f value, the decay of the amplitude of the pitching and plunging slows down until V_f reaches some critical value when the amplitude of the airfoil motion stays constant as shown in Fig. 16 when V_f = 1.10. At higher V_f, the motion of the airfoil will diverge as shown in Fig. 17, in which V_f is 1.20.

From the figures above, we see that the displacements of the airfoil motion predicted by using the simplified boundary conditions agree well with those by using the accurate boundary conditions for both the stable and unstable cases. In particular, Fig. 16 shows that the amplitude of the pitching and plunging by the two different boundary condition methods coincide with each other for the neutral stability case.

Based on the above results, the flutter boundary is predicted by both the simplified boundary conditions and accurate boundary conditions. The stability boundary is shown in Fig. 18. The results from the two different boundary conditions are compared with the results from Alonso et al.[16] and Liu et al.[13] The agreement is good and the transonic "dip" is predicted accurately. The results show that the simplified boundary conditions on stationary grids can predict the flutter cases with the same level of accuracy as those with the accurate boundary conditions.

Even though first-order approximation is used in the simplified boundary conditions, the method appears to be able to predict LCO (Limited Cycle Oscillation). Fig. 19 shows such a case at V_f = 1.33 and M_∞=0.75 for Isogai wing model. The amplitude with the simplified boundary conditions is a little bit higher than that with the accurate boundary conditions.

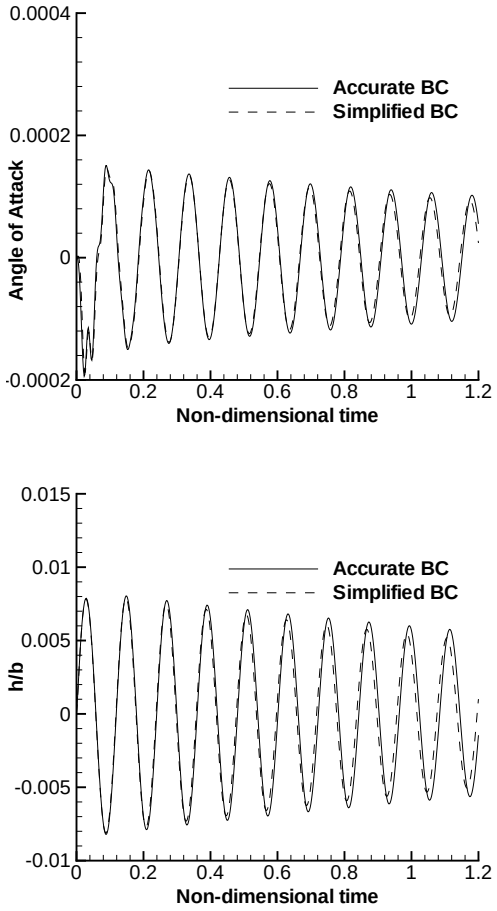

Fig. 15 Time history of pitching and plunging motion for Isogai wing model for $M_\infty = 0.750$ $\mathbf{V}_f = 1.00$.

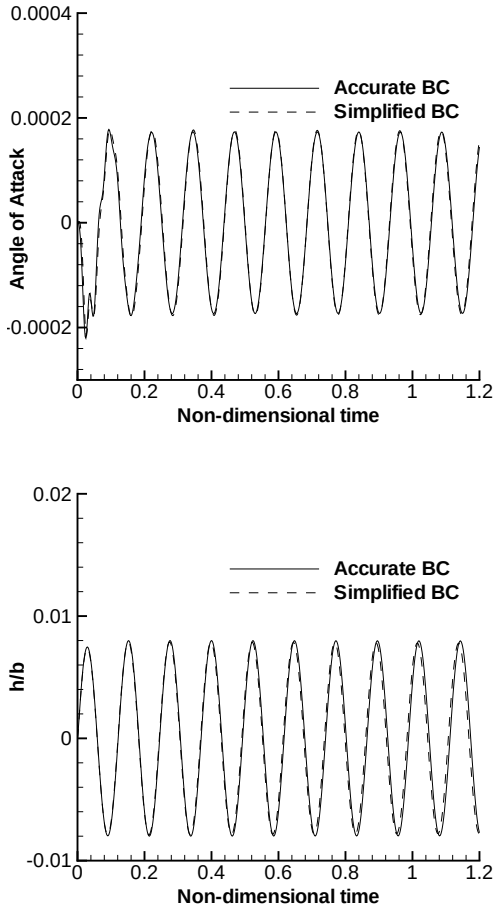

Fig. 16 Time history of pitching and plunging motion for Isogai wing model for $M_\infty = 0.750$, $\mathbf{V}_f = 1.10$.

V. Summary and Conclusion

Small perturbation boundary conditions are formulated for solving the unsteady Euler equations on body-conforming stationary grids. The CFD solver with the approximate boundary conditions is coupled with elastic equations to predict the aeroelastic properties of airfoils. During the aeroelastic computation process, the accurate nonlinear Euler equations are solved in the field, while the movements of the solid surfaces is accounted for in the new boundary conditions without moving or deforming the computational grids. The first-order wall boundary conditions are used in solving the full Euler equations for steady, unsteady and aeroelastic cases, and the results are compared with Euler solutions with full boundary conditions on moving grids and known experimental data. These results indicate that:

1. The relative error in surface pressure distribution for steady flows behaves linearly with both the thickness and the angle deviations from the nominal airfoil around which the approximate boundary conditions are obtained. The error is larger for transonic flows than for subsonic flows. If the thickness deformation is less than 50% and the rotation angle is less than 5 degrees, the relative error of the pressure as defined by eq. (15) is within 10%.

2. The approximate boundary condition method on non-moving grids are more accurate for unsteady flows than for steady flows because the motion of the airfoil is accurately represented in the approximate boundary conditions. Only the instantaneous location of the airfoil is approximated. A less than 5% error is incurred for airfoil rotation angles up to 20 degrees for the NACA64A010 airfoil at a transonic speed.

3. The simplified boundary conditions have been successfully used in CFD/CSD coupled simulation

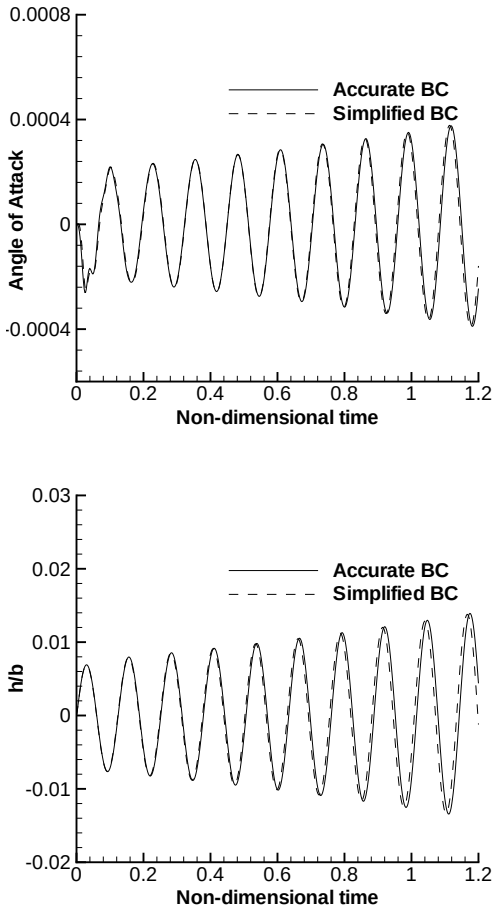

Fig. 17 Time history of pitching and plunging motion for Isogai wing model for $M_\infty = 0.750$, $\mathbf{V}_f$ = 1.20.

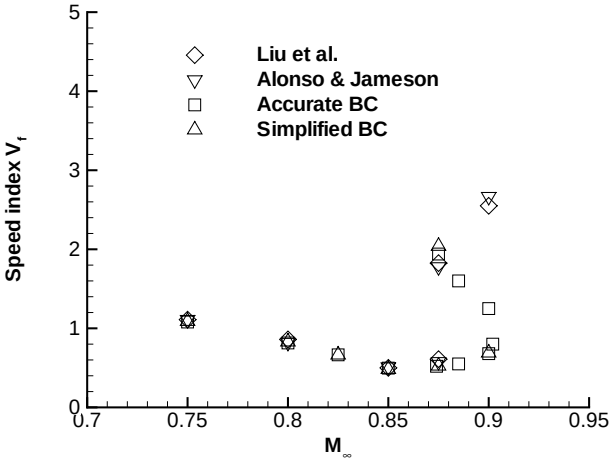

Fig. 18 Comparison of flutter boundary of NACA64A010.

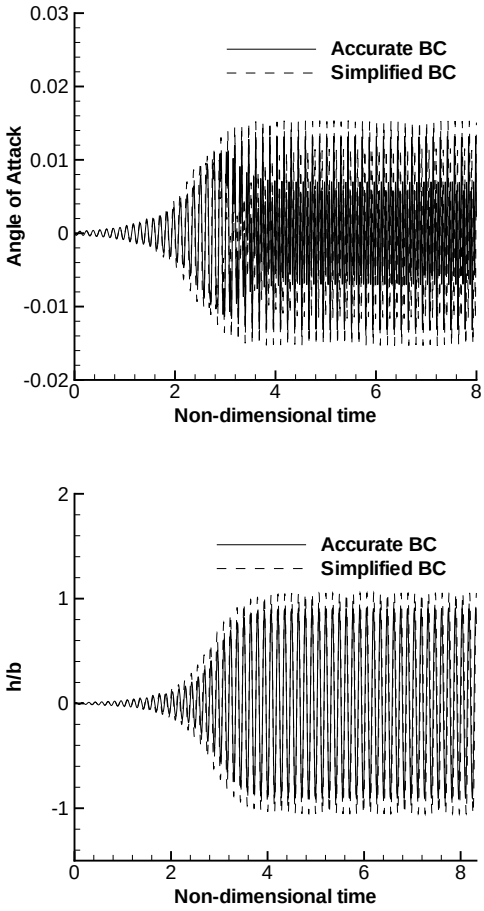

Fig. 19 Time history of pitching and plunging motion for Isogai wing model for M_∞=0.750, $\mathbf{V}_f$ =1.33.

of flutter of the airfoil. The computations using the first-order approximated boundary conditions accurately predicted the flutter boundary of the Isogai wing model compared to results by using the full boundary conditions on moving grids. LCO is also predicted except that the the amplitude of the displacement is a little bit higher than that with the accurate boundary conditions.

References

[1]Batina, J. T., "A Finite-Difference Approximate-Factorization Algorithm for Solution of the Unsteady Transonic Small-Disturbance Equation," NASA TP 3129, Jan. 1992.

[2]Edwards, J., "Transonic Shock Oscillations Calculated with a New Interactive Boundary Layer Coupling Method," AIAA Paper 93-0777, 1993.

[3]Edwards, J., "Transonic Shock Oscillations and Wing Flutter Calculated with an Interactive Boundary Layer Coupling Method," *EUROMECH-Colloquium 349, Simulation of Fluid-Structure Interaction in Aeronautics*, Gottingen, Germany, Sept. 1996.

[4]Gao, C., Luo, S., and Liu, F., "Calculation of Unsteady

Transonic Flow by an Euler Method with Small Perturbation Boundary Conditions," AIAA Paper 2003-1267, Jan. 2003.

[5]Gao, C., Luo, S., Liu, F., and Schuster, D. M., "Calculation of Airfoil Flutter by an Euler Method with Approximate Boundary Conditions," AIAA Paper 2003-3830, June 2003.

[6]Sankar, L., Malone, J., and Tassa, Y., "An Implicit Conservative Algorithm for Steady and Unsteady Three-Dimensional Transonic Potential Flows," AIAA Paper 1981-1016, June 1981.

[7]Sankar, L., Malone, J., and Schuster, D., "Euler Solutions for Transonic Flow Past a Fighter Wing," *Journal of Aircraft*, Vol. 24, No. 1, Jan. 1987, pp. 10–16.

[8]Fisher, C. C. and Andrew S. Arena, J., "Calculation of Airfoil Flutter by an Euler Method with Approximate Boundary Conditions," AIAA Paper 2003-3830, June 2003.

[9]Sadeghi, M., Yang, S., and Liu, F., "Parallel Computation of Wing Flutter with a Coupled Navier-Stokes/CSD Method," AIAA Paper 2003-1347, Jan. 2003.

[10]Liu, F. and Jameson, A., "Multigrid Navier-Stokes Calculations for Three-Dimensional Cascades," *AIAA Journal*, Vol. 31, No. 10, October 1993, pp. 1785–1791.

[11]Liu, F. and Ji, S., "Unsteady flow calculations with a multigrid Navier-Stokes method," *AIAA Paper 95-2205*, June 1995.

[12]Davis, S. S., "NACA64A010 Oscillatory Pitching," Compendium of Unsteady Aerodynamics Measurements, AGARD Report 702, 1982.

[13]Liu, F., Cai, J., Zhu, Y., Wong, A. S. F., and Tsai, H.-M., "Calculation of Wing Flutter by a Coupled Fluid-Structure Method," *Journal of Aircraft*, Vol. 38, No. 2, Mar.-Apr. 2001, pp. 334–342.

[14]Isogai, K., "On the Transonic-Dip Mechanism of flutter of a Sweptback Wing," *AIAA Journal*, Vol. 17, No. 7, July 1979, pp. 793–795.

[15]Isogai, K., "On the Transonic-Dip Mechanism of flutter of a Sweptback Wing: Part II," *AIAA Journal*, Vol. 19, No. 9, Sept. 1981, pp. 1240–1242.

[16]Alonso, J. J. and Jameson, A., "Fully-Implicit Time-Marching Aeroelastic Solutions," AIAA Paper 94–0056, Jan. 1994.